Available online at www.sciencedirect.com

ScienceDirect

Geochimica et Cosmochimica Acta 149 (2015) 88–102

Geochimica et Cosmochimica Acta

www.elsevier.com/locate/gca

Evidence for nucleosynthetic enrichment of the protosolar molecular cloud core by multiple supernova events

Martin Schiller *, Chad Paton, Martin Bizzarro

Centre for Star and Planet Formation, University of Copenhagen, Øster Voldgade 5-7, DK-1350, Denmark

Received 17 March 2014; accepted in revised form 5 November 2014; available online 13 November 2014

Abstract

The presence of isotope heterogeneity of nucleosynthetic origin amongst meteorites and their components provides a record of the diverse stars that contributed matter to the protosolar molecular cloud core. Understanding how and when the solar system's nucleosynthetic heterogeneity was established and preserved within the solar protoplanetary disk is critical for unraveling the earliest formative stages of the solar system. Here, we report calcium and magnesium isotope measurements of primitive and differentiated meteorites as well as various types of refractory inclusions, including refractory inclusions (CAIs) formed with the canonical $^{26}Al/^{27}Al$ of $\sim 5 \times 10^{-5}$ (^{26}Al decays to ^{26}Mg with a half-life of $\sim$0.73 Ma) and CAIs that show fractionated and unidentified nuclear effects (FUN-CAIs) to understand the origin of the solar system's nucleosynthetic heterogeneity. Bulk analyses of primitive and differentiated meteorites along with canonical and FUN-CAIs define correlated, mass-independent variations in ^{43}Ca, ^{46}Ca and ^{48}Ca. Moreover, sequential dissolution experiments of the Ivuna carbonaceous chondrite aimed at identifying the nature and number of presolar carriers of isotope anomalies within primitive meteorites have detected the presence of multiple carriers of the short-lived ^{26}Al nuclide as well as carriers of anomalous and uncorrelated ^{43}Ca, ^{46}Ca and ^{48}Ca compositions, which requires input from multiple and recent supernovae sources. We infer that the solar system's correlated nucleosynthetic variability reflects unmixing of old, galactically-inherited homogeneous dust from a new, supernovae-derived dust component formed shortly prior to or during the evolution of the giant molecular cloud parental to the protosolar molecular cloud core. This implies that similarly to ^{43}Ca, ^{46}Ca and ^{48}Ca, the short-lived ^{26}Al nuclide was heterogeneously distributed in the inner solar system at the time of CAI formation.

1. INTRODUCTION

Giant molecular clouds (GMC) constitute the densest part of the interstellar medium (ISM) and are the primary reservoirs of gas and dust in the galaxy. Interstellar dust grains incorporated into GMCs include amorphous silicate, amorphous carbon, silicon carbide and possibly crystalline silicates, which have been produced in diverse stellar environments and processed within the interstellar medium. GMCs are the primary site of star formation and it is well established that low-mass stars like our Sun are formed in clusters within these environments (Fukui and Kawamura, 2010; Kennicutt and Evans, 2012). Astronomical observations and numerical simulations of star-forming complexes suggest that GMCs have typical lifetimes of a few tens of Ma (Murray, 2011), during which multiple episodes of massive star formation may take place (Vasileiadis et al., 2013). Massive stars within GMCs provide the main energy source for the ISM, partly by destroying their birth clouds and polluting their nearby environments with freshly-synthesized matter (Matzner, 2002). Therefore, the nucleosynthetic make-up of a protostellar core is expected to reflect a mixture of an old galactically-inherited component with younger supernova-derived material produced during the lifetime of the GMC.

* Corresponding author.
E-mail address: Schiller@snm.ku.dk (M. Schiller).

http://dx.doi.org/10.1016/j.gca.2014.11.005
0016-7037/

Meteorites and their components provide a unique window into the processes leading to the earliest formative stages of the solar system, including the evolving nucleosynthetic make-up of the dense molecular cloud fragment from which our Sun formed. Indeed, earlier studies of meteorites have established the presence of now extinct, supernova-derived, short-lived ($t_{1/2}$ < 10 Ma) radionuclides (e.g., ^{41}Ca, ^{26}Al, ^{60}Fe, ^{53}Mn, ^{182}Hf) during the early solar system evolution (Lee et al., 1977; Srinivasan et al., 1994; Bizzarro et al., 2004; Trinquier et al., 2008; Kleine et al., 2009; Krot et al., 2009; Schiller et al., 2010), leading to the simple model that the solar system formed in the vicinity of a single dying massive star. Although, the solar system initial abundances of some of these isotopes has been recently challenged (e.g., Liu et al., 2012; Tang and Dauphas, 2012), their presence still requires that a young component formed shortly prior to the formation of our solar system and was incorporated into the protosolar molecular cloud. On the other hand, the preservation in primitive meteorites of presolar grains believed to have formed in the outflows of asymptotic giant branch (AGB) stars (Zinner, 2007; Davis, 2011) suggest an older, galactically-inherited, dust component formed before the isolation of the GMC is also present amongst the dust within the presolar molecular cloud core. Of particular interest is the presence of nucleosynthetic isotope heterogeneity that exists amongst inner solar system solids, planets, and asteroids, most noticeably for neutron-rich isotopes of the iron-group elements such as ^{48}Ca, ^{50}Ti, ^{54}Cr, and ^{64}Ni (Lee et al., 1978; Lee et al., 1979; Jungck et al., 1984; Niederer and Papanastassiou, 1984; Ireland et al., 1992; Birck, 2004; Trinquier et al., 2007; Trinquier et al., 2009; Moynier et al., 2010; Chen et al., 2011; Qin et al., 2011a,b; Zhang et al., 2011; Huang et al., 2012; Steele et al., 2012). Although originally interpreted to reflect incomplete mixing of presolar components following collapse of the protosolar molecular cloud (Rotaru et al., 1992; Birck, 2004), a number of studies now recognize that isotope anomalies of nuclides with distinct nucleosynthetic origins are correlated amongst bulk solar system reservoirs (Clayton et al., 1988; Trinquier et al., 2009; Qin et al., 2011a; Burkhardt et al., 2012; Paton et al., 2013). This suggests that the correlated variability does not represent initial disk heterogeneity, but instead unmixing of nucleosynthetic components during the earliest stages of solar system formation perhaps via thermal processing of molecular cloud material associated with volatile-element depletions in the inner solar system (Trinquier et al., 2009). However, other authors have argued that the correlated variability is best explained as a result of late addition of freshly-synthesized material from a nearby supernova into the presolar molecular cloud core or, alternatively, the solar protoplanetary disk (Dauphas et al., 2010; Qin et al., 2010). Distinguishing between these two classes of models is an important step towards a better understanding of the astrophysical environment of solar system formation and, hence, the birthplace of the Sun.

We identified Ca as an ideal element to probe the origin of nucleosynthetic heterogeneity in our solar system, as it comprises six isotopes that are produced by distinct processes during hydrostatic and explosive nucleosynthesis in stars (Burbidge et al., 1957; Wallerstein et al., 1997; Clayton, 2003). In particular, low entropy freeze-out is responsible for the synthesis of nearly all ^{48}Ca in existence. This type of environment is typically only found in high density type Ia supernovae (Meyer et al., 1996), although recent work suggest that electron capture supernovae, a rare subset of type II supernovae arising from the collapse of AGB stars with O–Ne–Mg cores, could, in principle, also create an environment under which ^{48}Ca may be synthesized (Wanajo et al., 2013). However, common to both is that resulting ^{48}Ca abundances ejected from such stars are several orders of magnitudes higher than those of the other Ca isotopes (Wanajo et al., 2013) and, thus, ^{48}Ca is formed by a markedly distinct process compared to the remaining Ca isotopes, which are predominantly products of either stellar (helium-, oxygen- and silicon-burning) or type II supernova nucleosynthesis. Therefore, the presence of correlated Ca-isotope anomalies between bulk solar system reservoirs for nuclides with distinct nucleosyntheses provides a means of identifying the cause of the observed solar system's nucleosynthetic variability. To achieve this goal, it is also important to constrain the nature and number of presolar carriers of isotope anomalies in primitive meteorites. This information can be obtained through sequential acid dissolution of primitive carbonaceous chondrites, as this method provides a crude chemical separation of the mineralogically distinct presolar carriers (e.g., Rotaru et al., 1992; Podosek et al., 1997; Dauphas et al., 2002; Trinquier et al., 2007; Reisberg et al., 2009; Trinquier et al., 2009; Moynier et al., 2010; Paton et al., 2013). The time of formation of the presolar carrier(s) responsible for the nucleosynthetic heterogeneity can, in turn, be inferred from ^{26}Mg excesses related to the decay of the short-lived ^{26}Al radionuclide ($t_{1/2}$ = 0.73 Ma). For example, nucleosynthetic heterogeneity associated with the presence of ^{26}Mg excesses reflecting ^{26}Al decay would imply that these presolar carriers represent a young dust population produced during the lifetime of ^{26}Al.

Nucleosynthetic variability of Ca isotopes has previously been identified in presolar grains (e.g., Nittler et al., 1996), canonical and CAIs that show fractionated and unidentified nuclear effects (FUN; Wasserburg et al., 1977; Jungck et al., 1984; Niederer and Papanastassiou, 1984; Moynier et al., 2010; Huang et al., 2012), bulk solar system matter (Simon et al., 2009; Moynier et al., 2010; Chen et al., 2011) and by sequential acid dissolution of primitive meteorites (Moynier et al., 2010). However, the majority of these studies were focused on identifying ^{48}Ca effects in highly anomalous material such as presolar grains and FUN-type CAIs and, thus, the level of precision of these earlier measurements is too low to allow the detection of small differences in the Ca isotope composition of bulk meteorites. Although the precision of Ca isotope measurements has significantly improved with the advent of second generation thermal ionization mass spectrometers (Moynier et al., 2010; Chen et al., 2011), it is still not possible to detect potential anomalous ^{46}Ca compositions using these techniques given the low abundance of the ^{46}Ca nuclide (0.004%). To alleviate these shortcomings, we take advantage of newly-developed techniques (Bizzarro et al., 2011;

Schiller et al., 2012) to measure with unprecedented precision and accuracy the Ca and Mg isotope composition of strategically selected meteorites and meteoritic inclusions by multiple collector-inductively coupled plasma-mass spectrometry (MC-ICP-MS). In detail, we have measured bulk samples from thirteen meteorites that encompass the known range of ^{54}Cr and ^{50}Ti anomalies (Trinquier et al., 2007; Trinquier et al., 2009) in these types of materials. These data are supplemented by analysis of two U-corrected Pb–Pb dated calcium aluminum-rich refractory inclusions (CAIs) with canonical ^{26}Al abundances (31E and 32E; Larsen et al., 2011; Connelly et al., 2012) as well as two FUN-type CAIs (STP-1 and KT-1; Thrane et al., 2008; Holst et al., 2013), whose mineralogy and petrology are described in detail in the aforementioned references and in Krot et al. (2014). FUN CAIs are amongst solar system materials with the most extreme isotopic compositions for various elements (Birck, 2004). To better understand the number and isotopic composition of presolar carriers of isotope anomalies, we performed a sequential acid dissolution of a large sample of the CI chondrite Ivuna. CI chondrites are ideally-suited meteorites for this purpose because their matrix contains the highest abundance of presolar grains and, thus, CI chondrites are considered to be the least chemically altered meteorites (Huss et al., 2003). Our new data for bulk analysis of primitive and differentiated meteorites as well as canonical and FUN-type refractory inclusions define a single linear array in Ca isotope (^{43}Ca, ^{46}Ca, and ^{48}Ca) space. Because our sequential dissolution experiment has identified the presence of multiple mineralogically distinct carriers of ^{43}Ca, ^{46}Ca, and ^{48}Ca anomalies, the presence of correlated Ca isotope anomalies in bulk analysis is most consistent with unmixing of nucleosynthetic components during the early stages of solar system formation. The presence of ^{26}Mg excesses interpreted as reflecting ^{26}Al decay in mineralogical components containing Ca isotope anomalies suggests that the solar system's nucleosynthetic heterogeneity reflects a young dust component derived from multiple supernova events.

2. METHODS

Fresh fragments weighing approximately 10–100 mg were extracted from the interior parts of the meteorites and inclusions, crushed to a fine powder with an agate pestle and mortar, and digested with HF-HNO_3 acid mixtures in Teflon beakers on a hot plate at 130 °C. Approximately 2.8 g of the Ivuna CI chondrite was gently crushed to a fine powder and subjected to a stepwise dissolution procedure, similar to procedures described in earlier work on the same types of meteoritic samples (Rotaru et al., 1992; Trinquier et al., 2007; Trinquier et al., 2009). The detailed procedure utilized in our study is described in Table 1. Residues remaining after individual dissolution steps were not dried down before proceeding to the next step. As described in earlier work, the step wise dissolution procedure we utilize is aimed at providing a crude separation of different mineralogical components. With increasing number of dissolution steps, the progressive approach of the dissolution procedure aims to dissolve increasingly chemically more resilient mineral phases. Initial steps are expected to dissolve carbonates and sulfates, while the intermediate steps attack metals and silicates and the last and most aggressive dissolution steps are aimed to digest refractory minerals. Sr isotope data for the same dissolution steps has already been reported by Paton et al. (2013).

Ca was purified from the sample matrix by ion exchange chromatography based on a four step procedure described in Schiller et al. (2012), which ensures an efficient separation of Ca from the sample matrix. Following purification, Ca isotopes were measured with the Neptune multiple collector – inductively couples plasma – mass spectrometer (MC-ICPMS) at the Natural History Museum of Denmark and detailed analytical procedures can be found in Schiller et al. (2012). Samples were aspirated into the plasma source by means of an Apex sample introduction system with an uptake rate of ~50 μL/min and Ca isotopes were measured with a mass resolving power (M/ΔM as defined by the peak edge width from 5% to 95% full peak height) that was always greater than 5000. The sensitivity under these analytical conditions was between 300 and 800 V ppm^{-1} and samples were analyzed with a signal intensity of approximately 100 V on mass ^{44}Ca, corresponding to a total signal strength of around 5000 V for a solution with a concentration of 8–16 ppm. Single analyses comprised a total of 839 s of data acquisition and 1000 s of baseline and each sample of sufficient size was systematically analyzed ten times relative to the SRM 915b standard. All data reduction was conducted off-line using the freely distributed Iolite data reduction package which runs within Igor Pro (Paton et al., 2011) and changes in mass bias with time were interpolated using a smoothed cubic spline. For each analysis the mean and standard error of the measured ratios were calculated, using a 3 sd threshold to reject outliers. Individual analyses of a sample were combined to produce an average weighted by the propagated uncertainties of individual analyses and reported final uncertainties are 2 times the standard error (2 se) of the mean. Ca mass-dependent isotope data are reported in the δ-notation as relative deviations from the SRM915b standard according to the formula:

$$\delta^{X}\mathrm{Ca} = \left[\frac{\left(^{X}\mathrm{Ca}/^{44}\mathrm{Ca}\right)_{\mathrm{sample}}}{\left(^{X}\mathrm{Ca}/^{44}\mathrm{Ca}\right)_{\mathrm{SRM915b}}} - 1\right] \times 10^{3}. \quad (1)$$

The mass-independent component in ^{43}Ca, ^{46}Ca, and ^{48}Ca is reported in similar fashion but in the μ-notation according to the following formula:

$$\mu^{X}\mathrm{Ca} = \left[\frac{\left(^{X}\mathrm{Ca}/^{44}\mathrm{Ca}\right)_{\mathrm{sample}}}{\left(^{X}\mathrm{Ca}/^{44}\mathrm{Ca}\right)_{\mathrm{SRM915b}}} - 1\right] \times 10^{6}, \quad (2)$$

and represents the deviations from the internally normalized ^{43}Ca/^{44}Ca, ^{46}Ca/^{44}Ca, and ^{48}Ca/^{44}Ca of the sample from the reference standard, normalized to a ^{42}Ca/^{44}Ca ratio of 0.31221 (Russell et al., 1978) using the exponential mass fractionation law. The external reproducibility for the mass-independent components reported as μ^{43}Ca, μ^{46}Ca, and μ^{48}Ca are estimated to be 1.8, 45 and 12.5 ppm, respectively, whereas the estimated external reproducibility of the

Table 1
Dissolution procedure for Ivuna.

Dissolution step	Solvent	T [°C]	time
L1	H_2O	20	30 min
L2	0.4 M Acetic acid	20	30 min
L3	8.5 M Acetic acid	20	24 h
L4	0.5 M HNO_3	20	10 min
L5	1 M HNO_3	20	1 h
L6	4 M HNO_3	20	24 h
L7	8 M HNO_3	20	24 h
L8	6 M HCl	20	24 h
L9	6 M HCl	130	24 h
L10	3 M HCl, 13 M HF	130	96 h
L11	17 M HF + 16 M HNO_3	130	240 h
L12	17 M HF + 16 M HNO_3, pressure bomb	150	24 h

mass-dependent isotope data is 0.05‰, 0.03‰, 0.10‰, and 0.10‰ for $\delta^{42}Ca$, $\delta^{43}Ca$, $\delta^{46}Ca$, and $\delta^{48}Ca$, respectively (Schiller et al., 2012).

In addition to Ca, the dissolution steps were also analyzed for Mg isotopes. Mg was separated from the matrix in a six step exchange resin procedure following the method described in Bizzarro et al. (2011). The isotopic composition of the purified Mg was determined using the Neptune MC-ICPMS at the Natural History Museum of Denmark and full analytical procedures are reported in Bizzarro et al. (2011). Samples were aspirated into the plasma source by means of an Apex sample introduction system with an uptake rate of ~50 μL/min, and the Mg isotope composition was measured in high resolution mode ($M/\Delta M > 5000$). Using this approach, the sensitivity of the instrument was ~200 V ppm^{-1} and samples were typically analyzed with a signal intensity of 100 V on mass ^{24}Mg. Single analyses comprised 1667 s of data acquisition and each sample was bracketed by standard analyses and systematically analyzed ten times. Mg isotope data are reported in the μ-notation as relative deviations from the DTS-2b standard ($\mu^{25}Mg_{DSM\text{-}3} = -122 \pm 17$ ppm (2 sd), Bizzarro et al., 2011) according to the following formula:

$$\mu^{X}Mg = \left[\frac{\left(^{X}Mg/^{24}Mg\right)_{sample}}{\left(^{X}Mg/^{24}Mg\right)_{DTS-2b}} - 1\right] \times 10^{6} \quad (3)$$

The mass-independent component in ^{26}Mg ($\mu^{26}Mg^{*}$) is reported in the same fashion, but represents deviations from the internally normalized $^{26}Mg/^{24}Mg$ of the sample from the reference standard, normalized to $^{25}Mg/^{24}Mg = 0.126896$ using the exponential mass fractionation law. Identical to Ca isotopes, all Mg data reduction was conducted off-line using the freely distributed Iolite data reduction package which runs within Igor Pro (Paton et al., 2011) and changes in mass bias with time were interpolated using a smoothed cubic spline. For each analysis the mean and standard error of the measured ratios were calculated, using a 3 sd threshold to reject outliers. Individual analyses of a sample were combined to produce an average weighted by the propagated uncertainties of individual analyses and reported final uncertainties are the 2 se of the mean. The external reproducibility $\mu^{26}Mg^{*}$ and $\mu^{25}Mg$ is estimated to be ~2.5 and ~20 ppm, respectively (Bizzarro et al., 2011). Reported $^{27}Al/^{24}Mg$ ratios of the individual dissolution steps were determined on unprocessed aliquots by a X-series 2 ICPMS at the Natural History Museum of Denmark and have an estimated external reproducibility of 5%.

3. RESULTS

In agreement with Valdes et al. (2014) little variability in the mass-dependent Ca isotope composition of non-carbonaceous primitive and differentiated meteorites exists, while carbonaceous chondrites, as represented here by Ivuna ($\delta^{42}Ca = 143 \pm 43$ ppm; Table 2), appear to be slightly enriched in the light isotopes of Ca. The canonical and FUN-type CAIs are characterized by large mass-dependent Ca isotope fractionation. Both canonical CAIs are enriched in light Ca isotopes of a magnitude similar to those reported by Huang et al. (2012), while the two FUN CAIs show both an enrichment (STP-1) and a depletion (KT-1) in their light Ca isotopes.

Our new high-precision mass-independent Ca isotope data for solar system reservoirs represented by primitive and differentiated meteorites as well as refractory inclusions demonstrate the presence of correlated excesses and deficits in $\mu^{43}Ca$, $\mu^{46}Ca$ and $\mu^{48}Ca$ relative to the terrestrial composition when using $^{42}Ca/^{44}Ca$ to correct for instrumental mass fractionation (Fig. 1, Table 2). In bulk samples, the $\mu^{43}Ca$ ranges from -7.3 ± 2.3 ppm in the eucrite Juvinas to $+11.5 \pm 1.4$ ppm in the ungrouped achondrite NWA 2976 whereas the $\mu^{46}Ca$ varies from -157 ± 33 ppm in the winonaite Tierra Blanca to $+96 \pm 35$ ppm in CI Ivuna chondrite. Similarly, the $\mu^{48}Ca$ ranges from -153.0 ± 5.0 ppm in the ureilite Kenna up to $+284.9 \pm 10.0$ ppm in the ungrouped achondrite NWA 2976, in broad agreement with earlier reports for differentiated meteorites (Chen et al., 2011). The canonical and FUN-type CAIs are characterized by the largest excesses and deficits, respectively, for all analyzed Ca isotopes. In detail, the 31E and 32E canonical CAIs have identical $\mu^{43}Ca$, $\mu^{46}Ca$ and $\mu^{48}Ca$ of $+30.0 \pm 1.8$, $+172 \pm 32$ and $+442.0 \pm 8.8$ ppm, respectively (Table 2). The STP-1 and KT-1 FUN CAIs have indistinguishable $\mu^{43}Ca$ and $\mu^{46}Ca$ deficits that average -206.3 ± 1.9 and -1109 ± 32 ppm, respectively, whereas their $\mu^{48}Ca$ deficits are -3498 ± 11 and -3307.0 ± 7.2 ppm, respectively.

Table 2
Ca isotope data for bulk samples and CAIs as well as individual steps of the dissolution experiment on the CI chondrite Ivuna.

Sample	Type	$\mu^{43}Ca$ (ppm)	$\mu^{46}Ca$ (ppm)	$\mu^{48}Ca$ (ppm)	$\delta^{42}Ca$ (‰)	$\delta^{43}Ca$ (‰)	$\delta^{46}Ca$ (‰)	$\delta^{48}Ca$ (‰)	Ca (rel.%)
Kenna	Ureilite	−3.4 ± 1.2	−1 ± 15	−153.0 ± 5.0	−0.208 ± 0.012	−0.107 ± 0.006	+0.192 ± 0.015	+0.234 ± 0.027	
Sahara 98505	Ureilite	−3.2 ± 1.8	−82 ± 32	−139.4 ± 5.5	−0.241 ± 0.031	−0.121 ± 0.015	+0.119 ± 0.051	+0.336 ± 0.059	
Juvinas	Eucrite	−7.3 ± 2.3	−20 ± 19	−91.5 ± 7.1	−0.124 ± 0.034	−0.068 ± 0.019	+0.089 ± 0.034	+0.160 ± 0.068	
Stannern	Eucrite	−4.0 ± 1.4	−41 ± 22	−102.4 ± 4.3	−0.094 ± 0.024	−0.051 ± 0.012	+0.059 ± 0.045	+0.078 ± 0.046	
Dorbigny	Angrite	−4.8 ± 1.0	+13 ± 17	−85.3 ± 7.5	−0.072 ± 0.018	−0.041 ± 0.010	+0.079 ± 0.032	+0.037 ± 0.024	
Sahara 99555	Angrite	−4.5 ± 1.5	−5 ± 57	−93.6 ± 6.6	−0.166 ± 0.077	−0.086 ± 0.038	+0.152 ± 0.105	+0.221 ± 0.140	
Bovedy	L3 chondrite	+1.3 ± 1.9	−3 ± 19	−35.4 ± 2.9	−0.128 ± 0.012	−0.063 ± 0.007	+0.125 ± 0.014	+0.188 ± 0.020	
Tierra Blanca	Winonaite	−2.0 ± 2.5	−157 ± 33	−21.3 ± 8.6	+0.127 ± 0.012	+0.060 ± 0.007	−0.279 ± 0.030	−0.266 ± 0.021	
Earth(n = 6)[1]		−0.7 ± 0.7	+5 ± 14	−0.2 ± 3.8	−0.061 ± 0.020	−0.029 ± 0.011	+0.067 ± 0.036	+0.113 ± 0.042	
Ivuna	CI chondrite	+11.3 ± 1.4	+96 ± 35	+206.1 ± 8.5	+0.143 ± 0.043	+0.081 ± 0.018	−0.081 ± 0.055	−0.069 ± 0.085	
NWA 2976	Ungrouped	+11.5 ± 1.4	+32 ± 45	+284.9 ± 10	+0.168 ± 0.045	+0.093 ± 0.024	−0.076 ± 0.112	−0.033 ± 0.080	
Refractory inclusions									
32E	Canonical CAI	+29.1 ± 2.0	+190 ± 12	+449.6 ± 5.3	+2.187 ± 0.047	+1.107 ± 0.023	−1.882 ± 0.064	−3.633 ± 0.090	
31E	Canonical CAI	+30.9 ± 1.8	+154 ± 26	+434.3 ± 9.0	+0.911 ± 0.051	+0.479 ± 0.024	−0.688 ± 0.062	−1.236 ± 0.116	
STP-1	FUN CAI	−206.0 ± 2.8	−1140 ± 52	−3498 ± 11	+1.645 ± 0.019	+0.607 ± 0.008	−2.710 ± 0.066	−6.548 ± 0.054	
KT-1	FUN CAI	−206.5 ± 2.0	−1078 ± 12	−3307 ± 7.2	−1.247 ± 0.008	−0.824 ± 0.004	+0.120 ± 0.014	−0.975 ± 0.016	
Ivuna dissolution steps									
L1		+5.4 ± 1.6	+30 ± 11	+209.2 ± 3.9	+0.044 ± 0.008	+0.027 ± 0.008	−0.004 ± 0.026	+0.102 ± 0.022	9.56
L2		+7.8 ± 0.9	+103 ± 9	+207.9 ± 3.6	+0.035 ± 0.024	+0.024 ± 0.013	+0.090 ± 0.026	+0.145 ± 0.047	24.52
L3		−7.1 ± 2.1	+99 ± 22	+226.9 ± 4.2	+0.098 ± 0.061	+0.041 ± 0.034	+0.010 ± 0.074	+0.300 ± 0.120	22.03
L4		+1.8 ± 1.4	−15 ± 20	+208.6 ± 8.2	+0.188 ± 0.024	+0.097 ± 0.012	−0.207 ± 0.038	−0.143 ± 0.049	36.46
L5		+5.9 ± 2.2	+84 ± 10	+206.1 ± 5.4	+0.060 ± 0.013	+0.033 ± 0.008	+0.025 ± 0.016	+0.094 ± 0.026	5.83
L6		+15.3 ± 4.0	+75 ± 20	+280 ± 12	+0.006 ± 0.038	+0.021 ± 0.021	+0.046 ± 0.040	+0.273 ± 0.075	0.54
L7		+37.7 ± 6.5	+170 ± 56	+995 ± 12	−0.430 ± 0.026	−0.170 ± 0.015	+0.593 ± 0.058	+1.790 ± 0.047	0.05
L8		+123.6 ± 6.5	+392 ± 60	+820 ± 15	+0.369 ± 0.012	+0.316 ± 0.009	+0.077 ± 0.060	+0.114 ± 0.022	0.10
L9		+18.1 ± 3.7	+214 ± 35	+626 ± 15	+0.300 ± 0.016	+0.161 ± 0.009	−0.080 ± 0.028	+0.066 ± 0.027	0.51
L10		+6.8 ± 4.2	+508 ± 30	+484 ± 14	+0.472 ± 0.009	+0.237 ± 0.007	+0.060 ± 0.029	−0.397 ± 0.015	0.30
L11		+242 ± 11	+2727 ± 150	+7850 ± 32	−0.252 ± 0.053	+0.126 ± 0.027	+2.996 ± 0.160	+8.314 ± 0.110	0.10

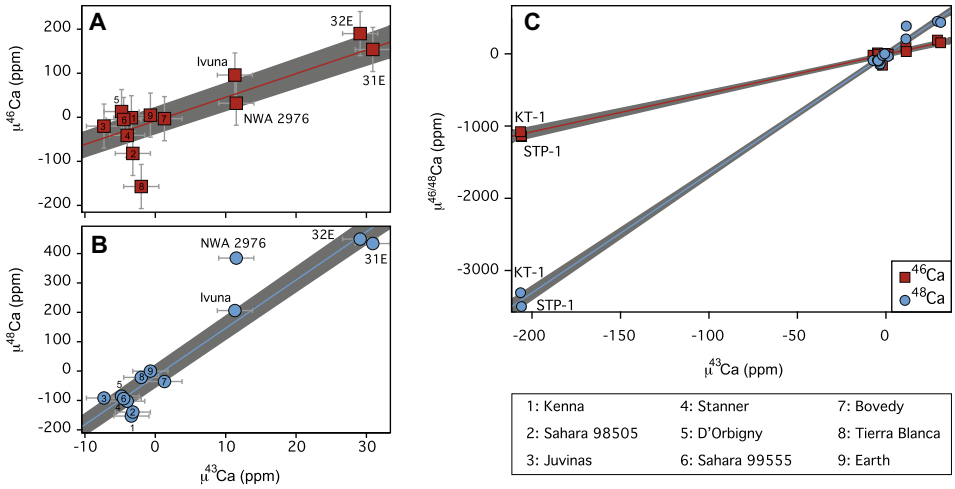

Fig. 1. Variation diagram of $\mu^{46}Ca$ (A) and $\mu^{48}Ca$ (B) versus $\mu^{43}Ca$ anomalies measured in measured achondrites, chondrites and CAIs. The same data are shown in (C) including data for FUN CAIs. The $\mu^{46}Ca$–$\mu^{43}Ca$ and $\mu^{48}Ca$–$\mu^{43}Ca$ correlation lines have an MSWD of 3.8 and 9.1 when including FUN CAIs. Excluding FUN inclusions returns similar MSWDs of 4.0 and 6.6 for the $\mu^{46}Ca$–$\mu^{43}Ca$ and $\mu^{48}Ca$–$\mu^{43}Ca$ correlation lines, respectively. Indicated in grey are the 95% confidence intervals of the regressions through all data and uncertainties shown for individual samples are the estimated external reproducibility of our data.

Analysis of the different dissolution steps of the Ivuna chondrite have identified the presence of multiple mineralogically distinct presolar carriers variably enriched in ^{43}Ca, ^{46}Ca, and ^{48}Ca. The $\mu^{43}Ca$ and $\mu^{46}Ca$ ranges from -7.1 ± 2.1 to $+242 \pm 11$ ppm and -15 ± 20 to $+2727 \pm 150$ ppm, respectively, and, in both cases, provides evidence for at least two distinct carriers in dissolution steps eight and eleven (Fig. 2). The early dissolution steps record $\mu^{43}Ca$ and $\mu^{46}Ca$ values that are significantly lower than the bulk Ivuna composition indicating that the variability observed in bulk solar system samples can be ascribed to selective incorporation of these two carriers in their precursor material. The $\mu^{48}Ca$ results differ in two important ways. First, the most anomalous ^{48}Ca compositions are present in step seven and eleven and, second, the $\mu^{48}Ca$ range of $+206.1 \pm 5.4$ to $+7850 \pm 32$ ppm fails to identify compositions that are resolvable lower than that of the bulk Ivuna chondrite. Taken at face value, our dissolution experiments provide evidence for at least three isotopically and mineralogically distinct presolar carriers of anomalous Ca in the CI Ivuna chondrite. Mg isotopes measured in the same sequential dissolution steps as for Ca isotopes also suggest the presence of three mineralogically distinct presolar carriers enriched in ^{26}Mg when the $^{25}Mg/^{24}Mg$ is used to correct for instrumental mass fractionation (Table 3). Apart from step four, which is not associated with the presence of an enriched Ca carrier, excess ^{26}Mg was also found in step eight and eleven, which are characterized by enrichments in $^{43,46}Ca$ and $^{43,46,48}Ca$, respectively. The Mg and Ca bulk isotopic compositions calculated by combining the individual dissolution steps are in agreement with the measured bulk composition (Tables 2 and 3; Larsen et al., 2011), indicating that our procedure successfully dissolved all Mg and Ca components.

4. DISCUSSION

4.1. Multiple presolar carriers of $\mu^{43}Ca$, $\mu^{46}Ca$, $\mu^{48}Ca$, and $\mu^{26}Mg^*$

The Ca isotope measurements presented here are internally normalized to the $^{42}Ca/^{44}Ca$ ratio to correct for instrumental mass fractionation during analysis and, therefore, it is possible that the anomalous compositions we report for the $\mu^{43}Ca$, $\mu^{46}Ca$ and $\mu^{48}Ca$ values of extraterrestrial materials may partially or predominately reflect ^{42}Ca and/or ^{44}Ca nucleosynthetic heterogeneity. Indeed, although ^{42}Ca is believed to be formed by both oxygen-burning and *s*-process nucleosynthesis, similarly to ^{43}Ca, an important contribution to the nucleosynthesis of ^{44}Ca comes from the decay of radioactive ^{44}Ti produced in supernovae (Nittler et al., 1996). Renormalizing our data for the sequential dissolution experiments reported in Fig. 2 to the $^{42}Ca/^{43}Ca$ ratio returns similar patterns for the ^{46}Ca and ^{48}Ca values but systematic depletions in ^{44}Ca. However, we emphasize that regardless of the ratio used for internal normalization, the overriding result emerging from our Ca isotope data is the presence of correlated nucleosynthetic heterogeneity amongst bulk solar solar system reservoirs for nuclides of distinct nucleosynthetic origins.

Of similar importance as the choice of the normalizing isotope ratio to avoid artificial mass-independent isotope effects, is the choice of the appropriate mass fractionation law that is used to correct intrinsic mass-dependent isotope fractionation in samples. Considering the high precision of the Ca isotope data, evaluation of the appropriate mass fractionation law becomes increasingly relevant even for samples that experienced little mass-dependent isotope

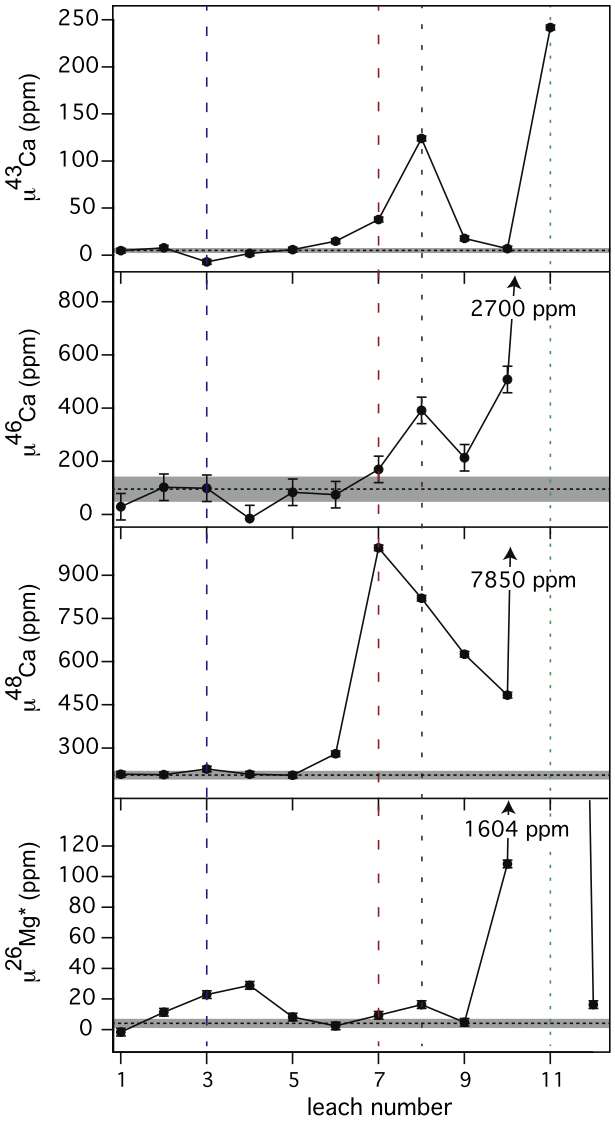

Fig. 2. Measured $\mu^{43}Ca$, $\mu^{46}Ca$, $\mu^{48}Ca$, and $\mu^{26}Mg^{*}$ of the stepwise dissolution experiment shown with increasing acid strength. Data that exceed the scale are marked by arrows. Vertical lines indicate the presence of a peak in one of the Ca isotopes interpreted as reflecting the dissolution of a pre-solar carrier phase in the leachate. Horizontal lines indicate the bulk Ivuna isotope composition. Bulk Mg isotope data is from Larsen et al. (2011).

fractionation. However, mass fractionation is particularly important for samples that experienced large mass-dependent isotope fractionation such as the canonical and FUN CAIs reported here. Recent laboratory experiments on the behavior of Ca during evaporation of perovskite in vacuum demonstrated that Ca isotope fractionation under these conditions follows a Rayleigh law (Zhang et al., 2014), while it appears that Ca isotope fractionation in CAIs can be explained by the exponential law (Huang et al., 2012). In an effort to decipher the appropriate mass fractionation law for the samples analyzed in this study, we monitored all possible fractionation laws using the generalized power law (GPL) as defined in Wombacher and Rehkämper (2003):

$$\mu^{i}Ca_{GPL} = \left(\frac{^{i}Ca}{^{44}Ca}\right)_{measured} \times f_{GPL}^{\left(m_i^n - m_{^{44}Ca}^n\right)}, \quad (4)$$

where m is the mass of the isotope and f_{GPL} is the fractionation coefficient:

$$f_{GPL} = \frac{\left(\frac{^{42}Ca}{^{44}Ca}\right)_{true}}{\left(\frac{^{42}Ca}{^{44}Ca}\right)_{measured}}^{\left(\frac{1}{m_{^{42}Ca}^n - m_{^{44}Ca}^n}\right)}. \quad (5)$$

The generalized power law is equivalent to the equilibrium, Rayleigh, exponential and power law when n equals -1, -0.5, $\rightarrow 0$, and $+1$, respectively. Correcting the canonical and FUN CAIs (i.e., the four samples with the largest mass-dependent isotope fractionation) using the different mass fractionation laws reveals that the calculated mass-independent component on $^{48}Ca/^{44}Ca$ determined for these inclusions can vary in each inclusion by several hundred ppm depending on which mass fractionation law is used for fractionation correction (Fig. 3). Although there is no explicit requirement for concordance in the mass-independent component for samples from these reservoirs, at least canonical CAIs appear to have a common nucleosynthetic signature in ^{50}Ti (Trinquier et al., 2009). For both canonical and FUN CAIs, the difference in the mass-independent $\mu^{48}Ca$ between the two samples of each type is smaller when using the exponential law than when correcting the data with the Rayleigh law. In particular, canonical CAIs have indistinguishable $\mu^{48}Ca$ signatures when using the exponential law for mass-dependent isotope fractionation. Thus, it appears that similar to Mg isotopes in canonical CAIs (Wasserburg et al., 2012), and contradictory to laboratory experiments, mass-dependent Ca isotope fractionation found in CAIs is best explained by the exponential law. Considering that the difference in the mass-dependent Ca isotope effects in the reported samples of differentiated and undifferentiated meteorites is generally more than an order of magnitude smaller than those between refractory inclusions, the effect of applying different mass fractionation laws is accordingly smaller and in most cases not resolvable at the level of our external reproducibility. Thus, all mass fractionation corrected data throughout this text is reported utilizing the exponential law.

The excesses in ^{26}Mg present in the stepwise dissolution steps could, similar to the Ca isotope data, reflect an anomalous ^{24}Mg or ^{25}Mg composition given that the $^{25}Mg/^{24}Mg$ ratio is used to correct for instrumental mass fractionation. Apparent excess of ^{26}Mg can arise through an anomalous composition of the ratio used for normalization, namely a composition deficient in ^{25}Mg. Although some rare presolar spinels are apparently characterized by ^{25}Mg deficits (Zinner et al., 2005), most of the Mg isotope anomalies present in solar system material are in the form of ^{26}Mg deficits observed in hibonite grains and FUN-type CAIs (Thrane et al., 2008; Liu et al., 2009; Holst et al., 2013). We note that the last step of the dissolution experiment, where these chemically resistant components are expected to be present, is characterized by a near terrestrial $\mu^{26}Mg$ value indicating that these potentially anomalous phases have little influence on the total $\mu^{26}Mg$ budget. Thus, we conclude that the most likely cause for the observed ^{26}Mg

Table 3
Mg isotope data for the individual steps of the dissolution experiment on the CI chondrite Ivuna.

Dissolution step	$\mu^{26}Mg^*$ (ppm)	$\mu^{45}Mg$ (ppm)	$\mu^{26}Mg$ (ppm)	$^{27}Al/^{24}Mg$	Mg (rel.%)
L1	−1.7 ± 1.0	−351 ± 7	−690 ± 10	0.000	8.93
L2	+12.1 ± 1.1	−509 ± 5	−980 ± 12	0.003	4.91
L3	+22.9 ± 1.2	−430 ± 7	−818 ± 14	0.045	7.65
L4	+28.9 ± 1.1	−331 ± 5	−624 ± 7	0.211	2.48
L5	+8.26 ± 0.9	−94 ± 5	−177 ± 9	0.123	5.87
L6	+2.5 ± 1.5	+86 ± 6	+174 ± 12	0.107	66.39
L7	+9.4 ± 1.4	+190 ± 10	+381 ± 18	0.124	2.73
L8	+16.4 ± 1.6	+77 ± 3	+167 ± 5	0.127	0.57
L9	+4.8 ± 1.4	+121 ± 6	+244 ± 12	0.131	0.20
L10	+108.3 ± 0.7	−19 ± 8	+73 ± 16	0.361	0.22
L11	+1604.3 ± 1.0	−985 ± 9	−327 ± 17	0.343	0.02
L12	+16.3 ± 1.3	−963 ± 14	−1864 ± 26	0.016	0.02

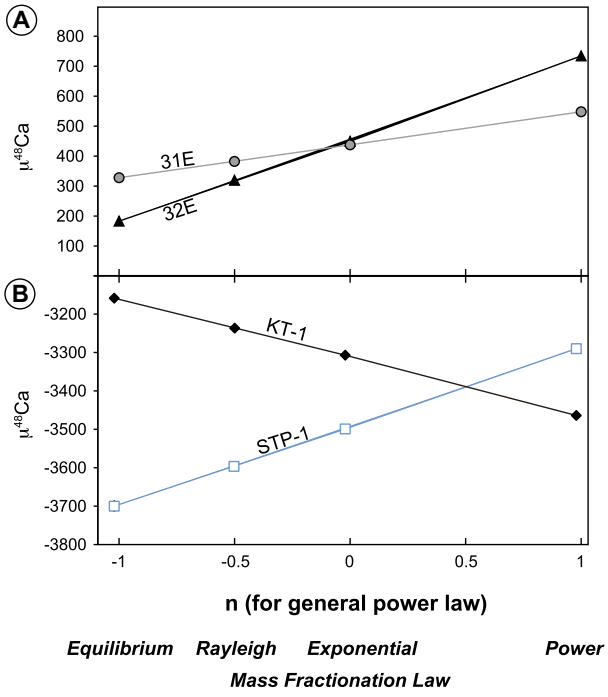

Fig. 3. Dependency of the calculated $\mu^{48}Ca$ for (A) the canonical CAIs 31E and 32E and (B) the FUN CAIs STP-1 and KT-1 on the mass fractionation law used to correct for mass-dependent isotope effects that result from the inherent large Ca stable isotope fractionation present in these refractory inclusions. The variable n is the exponent used in the generalized power law in Eqs. (4) and (5). The generalized power law is equivalent to the equilibrium, Rayleigh, exponential and power law when n equals −1, −0.5, →0, and +1, respectively. Uncertainties for $\mu^{48}Ca$ are smaller than the symbols.

excesses is the decay of the radioactive ^{26}Al nuclide, although it is not possible to asses whether the timing of this radioactive contribution to ^{26}Mg is recent or ancient.

The applied stepwise dissolution procedure is aimed at providing a crude chemical separation of the major mineralogical components of the bulk Ivuna chondrite. This is achieved by using acids and temperatures designed to target distinct mineralogical components. For example, initial dissolution steps are expected to dissolve sulfides, progressing to metal and silicate phases in later steps and, finally, the most chemically resistant phases such as spinels in the last and most aggressive steps. Therefore, individual dissolution steps are expected to contain multiple presolar carriers of similar mineralogy. For example, distinct generations of presolar silicates could populate dissolution step seven, which is designed to dissolve chemically reactive silicate minerals. The observation that enrichments in ^{26}Mg, ^{43}Ca, ^{46}Ca and ^{48}Ca are found in steps corresponding to different levels of acid resistance suggests the presence of multiple, mineralogically distinct carrier phases for the isotopically anomalous Mg and Ca compositions. An alternative explanation for the presence of multiple anomalous steps is that these reflect progressive or partial dissolution of a highly-anomalous chemically resistant phase. For example, the minor ^{48}Ca excesses present in step four and six could represent partial dissolution of a highly-anomalous chemically resistant phase dissolved in step eleven. However, the $\mu^{43}Ca$ and $\mu^{46}Ca$ ratios of the anomalous Ca in step three and seven are distinct from those of step eleven, indicating that the enrichment of ^{48}Ca observed in the earlier dissolution steps cannot represent partial dissolution of the highly-anomalous Ca present in step eleven, which may include a SiC component. We conclude that the variable Ca and Mg isotopic heterogeneity observed in the sequential dissolution experiments must reflect the presence of multiple presolar carriers.

We show in Fig. 4A–C the Ca isotopic composition of the stepwise dissolution experiment in relation to the correlated solar system variability defined by bulk meteorites, FUN CAIs and canonical CAIs. In $\mu^{46}Ca$–$\mu^{48}Ca$ space, the fractions with the greatest enrichments identified in the dissolution experiments (step eight, ten, and eleven) fall either on or very close to the solar system correlation line, with step eleven characterized by the most extreme enrichments and defining the ^{46}Ca–^{48}Ca-rich end-member of the correlation. This suggests that the bulk of the solar system's ^{46}Ca–^{48}Ca variability is controlled by a single carrier with a ^{46}Ca–^{48}Ca isotopic composition akin to step eleven. In this view, the two FUN CAIs analyzed here provide evidence for the existence of a complementary reservoir depleted in the ^{46}Ca–^{48}Ca carrier represented by step eleven. In

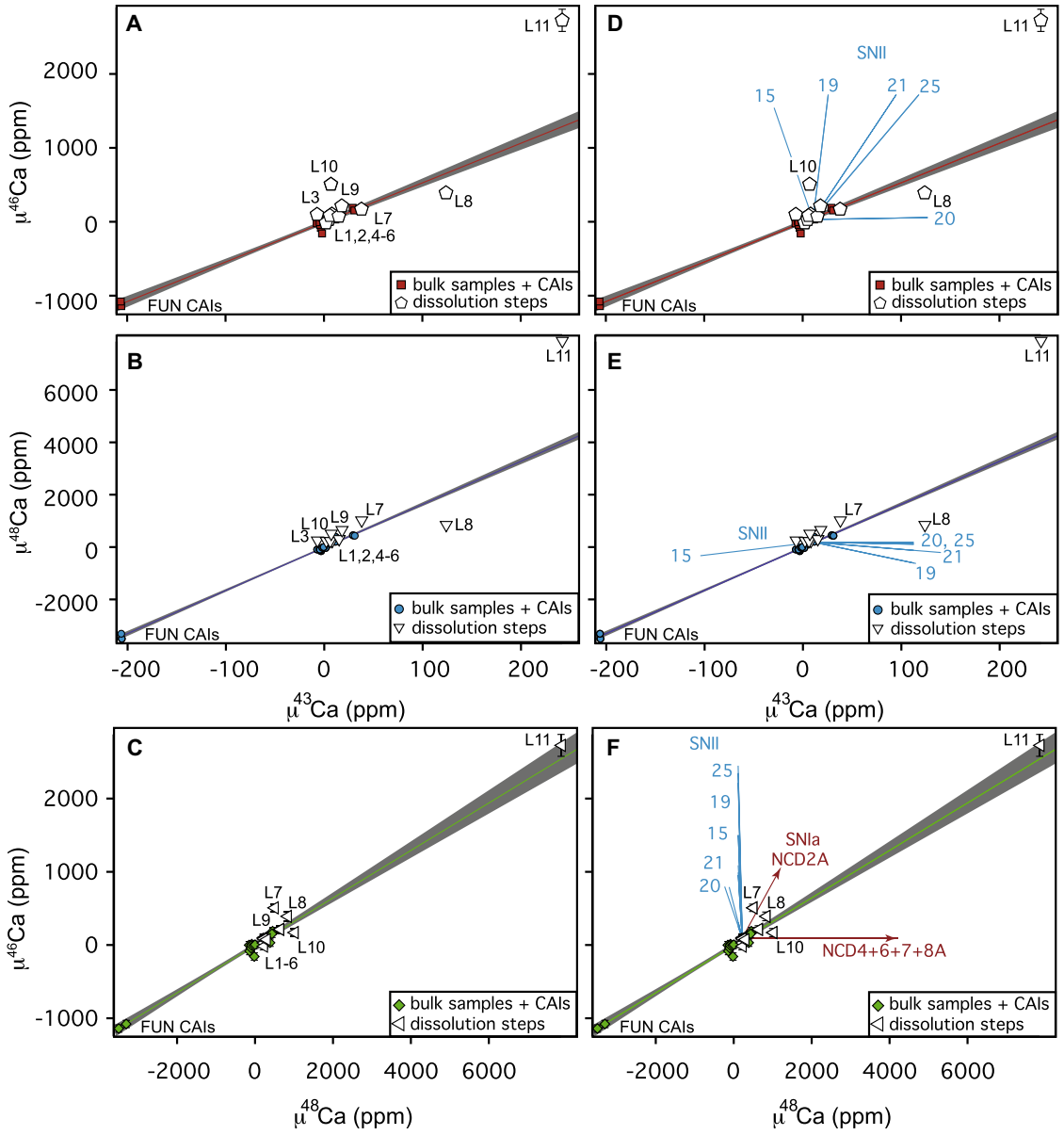

Fig. 4. $\mu^{46}Ca$–$\mu^{43}Ca$ (A) and $\mu^{48}Ca$–$\mu^{43}Ca$ (B) and $\mu^{46}Ca$–$\mu^{48}Ca$ (C) variation diagrams for the dissolution experiments shown together with data for bulk samples and CAIs. Dissolution step labels reflect individual dissolution steps. Panels (D–F) show mixing trajectories of CI type material with total yields of type II supernovae (blue) (Rauscher et al., 2002) and type Ia supernovae (red) (Woosley, 1997) with the bulk reservoir and dissolution experiment Ca isotope data. Numbers for type II supernovae indicate different progenitor mass in $M_{\odot}$ for models from Rauscher et al. (2002). For type Ia supernovae, the label reflects the model run, where the number is indicative of the density of the central zone at the time it first reaches 2×10^9 K (Woosley, 1997). Indicated in grey are the 95% confidence intervals of regressions through all bulk sample data. (For interpretation of the references to color in this figure legend, the reader is referred to the web version of this article.)

contrast, the isotopically enriched dissolution steps eight, ten, and eleven do not fall on the solar system correlation line in ^{46}Ca–^{43}Ca and ^{48}Ca–^{43}Ca space. This observation requires at least three distinct carriers to explain the observed variability, which can be approximated by the composition of dissolution steps eight, ten, and eleven. The scatter observed in the correlated variability of bulk solar system materials and refractory inclusions (Fig. 4) is consistent with the presence of multiple distinct carriers identified in the CI chondrite Ivuna.

4.2. Contamination of the presolar molecular cloud by multiple supernovae

As previously highlighted, individual dissolution experiments are expected to include a number of mineralogically similar carriers. These may reflect different populations of dust grains formed during a single supernova event or, alternatively, by distinct stars. As such, attempting to link the isotopic composition of our dissolution experiments with that of individual zones of a single supernova may

not provide a viable means to identify the nature of the star(s) responsible for the nucleosynthetic components present in Ivuna. Therefore, we first consider total stellar yields (Woosley, 1997; Rauscher et al., 2002) to compare in Fig. 4D–F the relative enrichment of ^{43}Ca, ^{46}Ca and ^{48}Ca in the dissolution experiments with that expected from type Ia supernovae of variable density as well as type II supernovae over a range of pre-explosive masses (15–25 $M_{\odot}$). The μ^{46}Ca–μ^{43}Ca, μ^{48}Ca–μ^{43}Ca and μ^{46}Ca–μ^{48}Ca variation diagrams indicate that the isotopic composition of the dissolution experiments cannot be explained by the ejecta of a single type Ia or II supernova. For example, while it is possible to explain the isotopic composition of dissolution step eleven by a 25 $M_{\odot}$ type II supernova in μ^{46}Ca–μ^{43}Ca space, ^{48}Ca is under-produced by this type of event such that a 25 $M_{\odot}$ type II supernova is not consistent the composition of step eleven in μ^{48}Ca–μ^{43}Ca space. Similarly, given that ^{43}Ca and ^{48}Ca are not co-produced in either type Ia or II supernovae, contributions from both these sources are required to account for the coupled ^{43}Ca and ^{48}Ca excesses present in dissolution step eleven. At face value, these observations imply that the Ca isotope compositions of the anomalous dissolution steps may reflect the cumulative effect of multiple supernova events, including both type Ia and II sources.

Despite the recent discovery of carriers of large ^{54}Cr isotope anomalies (Dauphas et al., 2010; Qin et al., 2011b), the existence of enrichments in the neutron-rich isotopes of iron group elements such as Ni, Cr and Ca has been recently challenged by Steele et al. (2012), arguing that these may instead reflect anomalies in the neutron-poor nuclides used for internal normalization when correcting for instrumental mass fractionation. If correct, this interpretation alleviates the need for an early solar system nucleosynthetic component containing matter produced by the quasi statistical equilibrium (QSE), which is efficiently produced and expelled from type Ia supernovae. However, in agreement with earlier work (e.g., Lee et al., 1979; Jungck et al., 1984), our Ca isotope data for bulk solar system materials and dissolution experiments do not support this proposal. First, the neutron-poor ^{40}Ca was not used for internal normalization and, second, the observed ^{48}Ca variability is present regardless of the internal normalization used to correct for instrumental mass fractionation. To further explore the nucleosynthetic origin of ^{54}Cr and ^{50}Ti, we show in Fig. 5 that the ^{48}Ca variability is positively correlated with ^{54}Cr and ^{50}Ti for the same samples and/or reservoirs. Given that ^{48}Ca is not expected to be efficiently expelled from core collapse (type II) supernova (Meyer et al., 1996), this observation suggests that at least part of the solar system's neutron-rich isotope heterogeneity stems from material either expelled from type Ia or rare electron capture type II supernova, which is the result of the explosion of a progenitor AGB star with an O–Ne–Mg core (Wanajo et al., 2009; Wanajo et al., 2013).

Steele et al. (2012) suggested that the solar system's Ni isotope heterogeneity observed for bulk meteorites cannot be explained from admixing of a component predominantly comprising debris from a single stellar source if the latter reflects the total stellar yields. In addition, these authors argue that the observed Ni isotope heterogeneity is best explained from material synthesized near the base of an SN II, namely the Si/S zone, with little pollution from the outer shells of the supernova. Using a similar approach, we compare in Fig. 6 the Ca isotope composition of the Ivuna leaches with that predicted for the various zones of a 25 $M_{\odot}$ type II supernova based on the model by Rauscher et al. (2002). The Ca isotope variability present in the leaches cannot be explained by a component dominated by material from the base of a type II supernova but instead from the intermediate shells, namely the O/Ne, O/C and He/C zones. This is in marked contrast to the interpretation of the source of the Ni isotope heterogeneity, as admixing of material from the O-producing zones from a type II supernova will dramatically perturb the final Ni isotopic composition of the ejected material (Steele et al., 2012). Moreover, we note that the existence of ^{26}Al-rich presolar carriers inferred from our data cannot be explained by contributions from the Ni and Si/S zones of a type II supernova, given that ^{26}Al is predominantly synthesized in the O/Ne zone (Woosley and Weaver, 1995). Therefore, it is apparent that a contrived scenario involving selective sampling of multiple zones is required to explain the solar system's isotope heterogeneity observed for a number of distinct nuclides if a single supernova source is invoked.

Given the evidence for contributions from at least two types of supernovae inferred from our Ca isotope data, we turn towards a possibly more plausible interpretation based on the current understanding of star forming regions. It is generally accepted that the majority of low mass stars form in dense clusters, namely in association with massive stars (Kennicutt and Evans, 2012). In particular, the close agreement of the Sun's abundance pattern with that of solar-twins in the M67 open cluster (Önehag et al., 2011) suggest that our solar system may have formed in a GMC giving rise to a similar high-mass cluster. A natural consequence of the temporal evolution of such a dynamical environment is the continuous pollution of the star-forming gas by freshly-synthesized nuclides produced and expelled from nearby massive stars. Indeed, recent numerical simulations of evolving GMCs suggest that, under typical star-forming conditions, the level of short-lived radionuclides such as ^{26}Al in star-forming gas resulting from continuous contamination from nearby massive stars is comparable to that of the early solar system (Vasileiadis et al., 2013). Therefore, the presence multiple carriers enriched in ^{43}Ca, ^{46}Ca, ^{48}Ca and ^{26}Al inferred from our dissolution experiment is most easily understood if these carriers reflect contamination of the proto-solar molecular cloud by diverse supernova sources shortly prior or during the lifetime of the GMC.

4.3. Excess of *r*-process isotopes in canonical CAIs

Although the observed correlation amongst bulk solar system reservoirs, canonical CAIs and FUN CAIs is generally good in Ca isotope space (Fig. 1), the positive correlation between ^{48}Ca and ^{50}Ti and ^{54}Cr is denatured by the observation that CAIs appear to contain an

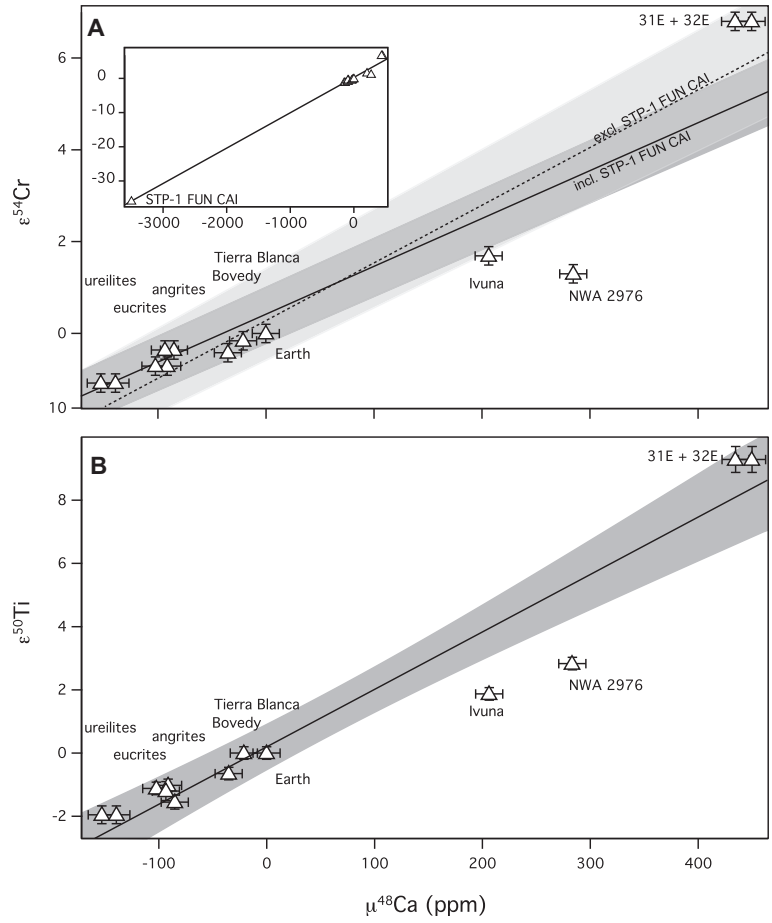

Fig. 5. ^{54}Cr–^{48}Ca (A) and ^{50}Ti–^{48}Ca (B) variation diagrams of primitive and differentiated meteorites as well as chondritic components reported in this study. ^{54}Cr and ^{50}Ti data are from Trinquier et al. (2007); Trinquier et al. (2009) and Holst et al. (2013). Indicated in grey are the 95% confidence intervals of the regressions.

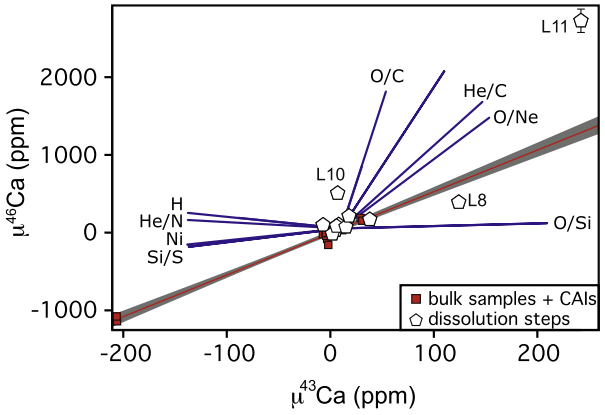

Fig. 6. Ca isotope variation diagram showing mixing trajectories of CI type material with yields from different zones of a 25 $M_{\odot}$ type II supernovae (Rauscher et al., 2002). Indicated in grey is the 95% confidence interval of the regression through all bulk sample data.

over-abundance of ^{50}Ti and ^{54}Cr compared to the remaining bulk solar system material (Fig. 5). It has been recently suggested that canonical CAIs present in CV chondrites contain an *r*-process excess for isotopes between mass 80 and 140 compared to a bulk solar system composition (Brennecka et al., 2013). Whereas ^{50}Ti and ^{54}Cr are efficiently produced by *r*-process nucleosynthesis, this is not the case for ^{48}Ca. Therefore, it is possible that the relatively enhanced abundance of ^{50}Ti and ^{54}Cr compared to the enrichment of ^{48}Ca in canonical CAIs is the result of the same process that led to the nucleosynthetic enrichment of *r*-process isotopes in the mass range 80 to 140 in these objects. If correct, this interpretation strengthens the idea that the nucleosynthetic make-up of ^{50}Ti and ^{54}Cr in canonical CAIs requires multiple stellar sources.

4.4. Unmixing of distinct dust populations?

The highly-anomalous isotopic composition of FUN CAIs observed for several elements is commonly cited as reflecting their formation from precursor material consisting of isotopically heterogeneous presolar aggregates (Sahijpal and Goswami, 1998). In this model, FUN CAIs formed from thermal processing of material that avoided isotopic homogenization through evaporation and condensation processes. However, the two FUN CAIs analyzed in our study fall

either on or very close to the correlation line defined by bulk solar system reservoirs and canonical CAIs, despite having large deficits in ^{43}Ca, ^{46}Ca and ^{48}Ca (Fig. 1) and this correlation persists independently of the chosen normalizing isotope (^{42}Ca, ^{43}Ca, or ^{44}Ca). This observation establishes that the extreme Ca isotopic composition recorded by FUN CAIs was imparted by a process similar to that responsible for the correlated isotope heterogeneity present in bulk solar system reservoirs, and not random sampling of isotopically heterogeneous presolar components. Given that our dissolution experiments have identified the existence of multiple mineralogically distinct presolar carriers of anomalous Ca in the Ivuna chondrite, it is unlikely that the correlated variability reported in Fig. 1 reflects an initially heterogeneous distribution of such carriers within the inner protoplanetary disk. This would require variable but proportional admixing of the different carriers amongst the precursor material of individual source reservoirs to maintain similar ^{46}Ca/^{43}Ca and ^{48}Ca/^{43}Ca ratios across the inner solar system. Rather, our results are supportive of a model where the correlated Ca isotope variability results from unmixing of initially physically well-mixed molecular cloud material.

The striking linearity observed in μ^{46}Ca–μ^{43}Ca and μ^{48}Ca–μ^{43}Ca for bulk analyses of primitive and differentiated meteorites as well as canonical and FUN CAIs requires that unmixing of the multiple presolar carriers identified by the dissolution experiments essentially behaves as a two component system. Based on a similar linear relationship for the ^{46}Ti and ^{50}Ti nuclides, Trinquier et al. (2009) proposed that the observed nucleosynthetic heterogeneity reflects thermal processing of molecular cloud material, which resulted in preferential loss by sublimation of thermally unstable and isotopically anomalous presolar carriers, producing residual isotopic heterogeneity. This model has been recently proposed to account for the solar system's Sr and Mo isotope heterogeneity observed in bulk solar system reservoirs (Burkhardt et al., 2012; Paton et al., 2013). A possibility is that the apparent two component mixing relationship predominately reflects the selective unmixing of two dust generations with contrasting thermal and/or physical properties. Our dissolution experiments have identified the presence of mineralogically distinct carrier phases with ^{26}Mg excesses that we interpret as reflecting decay of the ^{26}Al nuclide. Given the unequivocal evidence for live ^{26}Al during the early evolutionary stages of the solar system (Krot et al., 2009), this result suggests the presence of multiple presolar carriers of live ^{26}Al, which must represent a new dust component inherited shortly before or during collapse of the proto-solar molecular cloud. The mineralogical similarities between the carriers of Mg and Ca anomalies inferred from our dissolution experiments combined with the observation that nucleosynthetic anomalies in bulk solar system reservoirs are correlated with variations in the mass-independent ^{26}Mg composition (μ^{26}Mg*) – interpreted as reflecting ^{26}Al decay (Larsen et al., 2011) – implies that the carriers enriched in ^{43}Ca, ^{46}Ca and ^{48}Ca are all part of a new dust generation that formed close in time with the ^{26}Al-rich dust component. Therefore, we suggest that the solar systems correlated nucleosynthetic variability reflects the selective unmixing of old, galactically-inherited homogeneous dust from a new, supernovae-derived dust component formed shortly prior to or during the evolution of the GMC parental to the proto-solar molecular cloud core (Fig. 7). Unmixing can occur by thermal processing of ^{26}Al-rich in-falling dust during the earliest stages of solar system formation (Trinquier et al., 2009). This model implies that, similarly to ^{43}Ca, ^{46}Ca and ^{48}Ca, the short-lived ^{26}Al nuclide was heterogeneously distributed in the inner solar system at the time of CAI formation (Larsen et al., 2011). Given that the astrophysical sites for the efficient nucleosynthesis of ^{48}Ca are either a dense type Ia or a rare electron capture type II SN (Meyer et al., 1996; Woosley, 1997; Wanajo et al., 2013), this interpretation requires contribution from at least one supernova not typically associated with star forming regions to this unprocessed, young dust population. This can be achieved if, for example, a dense type Ia or a rare electron capture type II SN polluted the ambient interstellar medium shortly prior to the accumulation of the GMC.

Dust processing in the ISM results in erosion of the grain constituent atoms into the gas phase and is believed to occur through sputter in gas–grain collisions and vaporization during grain–grain collisions in supernova shock waves (Jones and Nuth, 2011). Although uncertain, current estimates of the silicate dust lifetime in the ISM are in the order of $\sim 1 \times 10^8$ years (Jones and Nuth, 2011), indicating that processing and destruction of dust in the ISM is rapid and efficient. Effective dust destruction implies the re-formation of local ISM dust populations, presumably from an isotopically homogenized gas of approximately "cosmic" composition. This is in line with observational constraints suggesting that most of the silicate dust in the ISM is amorphous (Kemper et al., 2004). As such, the bulk of the silicate dust accumulating in GMC complexes is expected to have experienced processing during a prior residence time in the ISM, resulting in

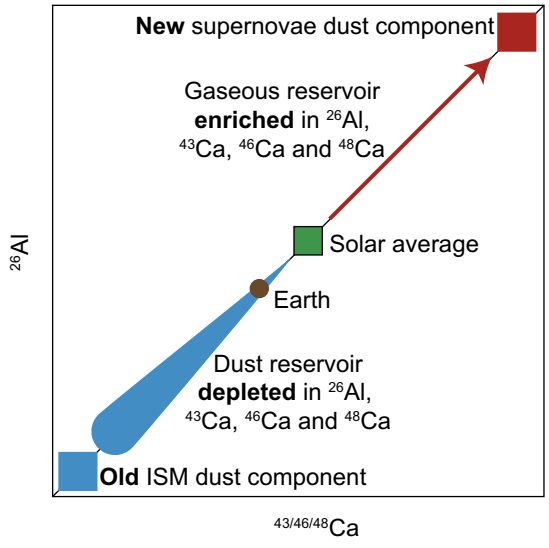

Fig. 7. Schematic diagram depicting the correlated isotope effects for ^{26}Al and ^{43}Ca, ^{46}Ca, and ^{48}Ca as a result of physical unmixing of 'old' dust inherited from the ISM and 'new' dust, recently produced by multiple supernovae shortly prior to or during the lifetime of the GMC.

its isotopic and chemical homogenization. A markedly distinct dust population may also exist in GMCs, reflecting a new dust component formed in the outflows of exploding massive stars shortly prior to or during the lifetime of the GMC. Indeed, recent infrared and submillimeter observations of the 1987A supernova remnant suggest efficient precipitation of SN ejectas in dust (Matsuura et al., 2011), implying that newly-formed dust must be a generic component of the ensemble of dust grains present in GMCs. Newly-formed and unprocessed SN dust is predicted to retain the isotopic composition of its source reservoir and, hence, is distinct from the ambient GMC dust. Selective unmixing of this isotopically anomalous dust component, perhaps by thermal processing (Trinquier et al., 2009), will lead to residual and correlated isotopic heterogeneity across solar system reservoirs.

Finally, we note that the decoupling between the initial abundances of the short-lived ^{182}Hf and ^{26}Al radionuclides in early-formed refractory inclusions is supportive of the model we propose for the origin of the isotopic heterogeneity existing in bulk solar system reservoirs (Holst et al., 2013). The STP-1 FUN inclusion analyzed here is characterized by large depletions in ^{43}Ca, ^{46}Ca and ^{48}Ca as well as a low initial ^{26}Al/^{27}Al of $2.94 \pm 0.21 \times 10^{-6}$. Yet, it records an initial ^{182}Hf abundance identical to that observed in CAIs with the canonical ^{26}Al/^{27}Al of $\sim 5 \times 10^{-5}$) (Larsen et al., 2011). This observation suggests that, in contrast to ^{43}Ca, ^{46}Ca, ^{48}Ca and ^{26}Al, the carrier of ^{182}Hf was well mixed within the Solar System's parental molecular cloud. Because ^{182}Hf is produced during the s-process in AGB stars that live significantly longer than the typical lifetime of giant molecular clouds (Lugaro et al., 2014; Murray, 2011), the initial ^{182}Hf abundance recorded by canonical and FUN CAIs must reflect a contribution from an older, galactically-inherited and isotopically homogenized dust component. The discovery of supernova-derived nanospinels with large ^{54}Cr enrichments in the matrix of the Orgueil carbonaceous chondrite (Dauphas et al., 2010; Qin et al., 2011b) is consistent with our proposal that a young, supernova-derived dust component was part of the protosolar molecular cloud assemblage.

5. CONCLUSIONS

A high-precision Ca and Mg isotope study of early solar system has shown that:

1. The Ca isotope composition of solar system reservoirs represented by primitive and differentiated meteorites as well as refractory inclusions (canonical and FUN CAIs) demonstrate the presence of correlated excesses and deficits in ^{43}Ca, ^{46}Ca and ^{48}Ca relative to the terrestrial composition when using the ^{42}Ca/^{44}Ca ratio to correct for instrumental mass fractionation. Collectively, the samples analyzed here define a single trend which we denote as the solar system Ca isotope correlation line.
2. Sequential acid dissolution experiments of the CI chondrite Ivuna aimed at identifying the nature and number of presolar carriers of isotope anomalies within primitive meteorites revealed the presence of at least three isotopically and mineralogically distinct carriers of anomalous and uncorrelated ^{43}Ca, ^{46}Ca and ^{48}Ca compositions. Likewise, Mg isotopes measured in the same sequential dissolution steps as for Ca isotopes suggest the presence of three mineralogically distinct presolar carriers enriched in ^{26}Mg when the ^{25}Mg/^{24}Mg is used to correct for instrumental mass fractionation. The most straightforward interpretation of the ^{26}Mg excesses is that they reflect decay of the radioactive ^{26}Al nuclide.
3. Comparing the Ca isotope compositions of individual acid dissolution experiments with total stellar yields from type Ia supernovae of variable density as well as type II supernovae over a range of pre-explosive masses (15 to 25 $M_{\odot}$) indicate that the isotopic composition of the dissolution experiments cannot be explained by the ejecta of a single type Ia or II supernova. Likewise, the presence of presolar carriers enriched in ^{26}Al coupled with the Ca isotopic variability observed in the dissolution experiments cannot be accounted for by stellar debris from the specific zone of a single 25 $M_{\odot}$ type II supernova. Therefore, the presence multiple carriers enriched in ^{43}Ca, ^{46}Ca, ^{48}Ca and ^{26}Al inferred from our dissolution experiment is most easily understood if these carriers reflect contamination of the proto-solar molecular cloud by diverse supernova sources.
4. The striking linearity of the solar system Ca isotope correlation line requires that unmixing of the multiple presolar carriers identified by the dissolution experiments essentially behaves as a two component system. A possibility is that the apparent two component mixing relationship predominately reflects the selective unmixing of two dust generations with contrasting thermal and/or physical properties. We propose that the solar system's correlated nucleosynthetic variability reflects the selective unmixing of old, galactically-inherited homogeneous dust from a new, supernovae-derived dust component formed shortly prior to or during the evolution of the GMC parental to the proto-solar molecular cloud core. Therefore, similarly to ^{43}Ca, ^{46}Ca and ^{48}Ca, the short-lived ^{26}Al nuclide was heterogeneously distributed in the inner solar system at the time of CAI formation.
5. The STP-1 and KT-1 FUN CAIs analyzed in our study fall either on or very close to the solar system Ca isotope correlation line defined by bulk solar system reservoirs and canonical CAIs, despite having large deficits in ^{43}Ca, ^{46}Ca and ^{48}Ca. This observation establishes that the extreme Ca isotopic composition recorded by FUN CAIs was imparted by a process similar to that responsible for the correlated isotope heterogeneity present in bulk solar system reservoirs, and not random sampling of isotopically heterogeneous presolar components.

ACKNOWLEDGEMENTS

Justin Simon, Andrew Davis, Typhoon Lee, one anonymous reviewer, and associated editor Shichun Huang provided comments that helped improve the manuscript. Research for this project was supported by a Danish National Research Foundation Centre of Excellence grant to M.B. (grant number DNRF97). M.B. further acknowledges funding from the European Research Council under

ERC Consolidator grant agreement 616027-STARDUST2ASTEROIDS.

REFERENCES

Birck J. -L. (2004) An overview of isotopic anomalies in extraterrestrial materials and their nucleosynthetic heritage. In *Reviews in Mineralogy and Geochemistry: Geochemistry of Non-Traditional Stable Isotopes* (eds. C.M. Johnson, B.L. Beard and F. Albarède). pp. 25–64.

Bizzarro M., Baker J. A. and Haack H. (2004) Mg isotope evidence for contemporaneous formation of chondrules and refractory inclusions. *Nature* **431**, 275–278.

Bizzarro M., Paton C., Larsen K., Schiller M., Trinquier A. and Ulfbeck D. (2011) High-precision Mg-isotope measurements of terrestrial and extraterrestrial material by HR-MC-ICPMS – Implications for the relative and absolute Mg-isotope composition of the bulk silicate Earth. *J. Anal. At. Spectrom.* **26**, 565–577.

Brennecka G. A., Borg L. E. and Wadhwa M. (2013) Evidence for supernova injection into the solar nebula and the decoupling of *r*-process nucleosynthesis. *Proc. Nat. Acad. Sci.* **110**, 17241–17246.

Burbidge E., Burbidge G., Fowler W. and Hoyle F. (1957) Synthesis of the elements in stars. *Rev. Mod. Phys.* **29**, 547–650.

Burkhardt C., Kleine T., Dauphas N. and Wieler R. (2012) Origin of isotopic heterogeneity in the solar nebula by thermal processing and mixing of nebular dust. *Earth Planet. Sci. Lett.*, 298–307.

Chen H.-W., Lee T., Lee D.-C., Jiun-San Shen J. and Chen J.-C. (2011) ^{48}Ca heterogeneity in differentiated meteorites. *Astrophys. J. Lett.* **743**, L23.

Clayton D. (2003). .

Clayton R., Hinton R. and Davis A. (1988) Isotopic variations in the rock-forming elements in meteorites. *Philos. Trans. R. Soc. Lond. Ser. A* **325**, 483–501.

Connelly J. N., Bizzarro M., Krot A. N., Nordlund Å., Wielandt D. and Ivanova M. A. (2012) The absolute chronology and thermal processing of solids in the solar protoplanetary disk. *Science* **338**, 651–655.

Dauphas N., Marty B. and Reisberg L. (2002) Molybdenum nucleosynthetic dichotomy revealed in primitive meteorites. *Astrophys. J.* **569**, L139–L142.

Dauphas N., Remusat L., Chen J. H., Roskosz M., Papanastassiou D. A., Stodolna J., Guan Y., Ma C. and Eiler J. M. (2010) Neutron-rich chromium isotope anomalies in supernova nanoparticles. *Astrophys. J.* **720**, 1577–1591.

Davis A. M. (2011) Stardust in meteorites. *Proc. Natl. Acad. Sci. USA* **108**, 19142–19146.

Fukui Y. and Kawamura A. (2010) Molecular clouds in nearby galaxies. *Ann. Rev. Astron. Astrophys.* **48**, 547–580.

Holst J. C., Olsen M. B., Paton C., Nagashima K., Schiller M., Wielandt D., Larsen K. K., Connelly J. N., Jørgensen J. K., Krot A. N., Nordlund Å. and Bizzaro M. (2013) ^{182}Hf–^{182}W age dating of a ^{26}Al-poor inclusion and implications for the origin of short-lived radioisotopes in the Early Solar System. *Proc. Natl. Acad. Sci. USA* **110**, 8819–8823.

Huang S., Farkaš J., Yu G., Petaev M. I. and Jacobsen S. B. (2012) Calcium isotopic ratios and rare earth element abundances in refractory inclusions from the Allende CV3 chondrite. *Geochim. Cosmochim. Acta* **77**, 252–265.

Huss G. R., Meshik A. P., Smith J. B. and Hohenberg C. M. (2003) Presolar diamond, silicon carbide, and graphite in carbonaceous chondrites: Implications for thermal processing in the solar nebula. *Geochim. Cosmochim. Acta* **67**, 4823–4848.

Ireland T. R., Zinner E. K., Fahey A. J. and Esat T. M. (1992) Evidence for distillation in the formation of HAL and related hibonite inclusions. *Geochim. Cosmochim. Acta* **56**, 2503–2520.

Jones A. P. and Nuth, III, J. A. (2011) Dust destruction in the ISM: A re-evaluation of dust lifetimes. *Astron. Astrophys.* **530**, A44.

Jungck M. H. A., Shimamura T. and Lugmair G. (1984) Ca isotope variations in Allende. *Geochim. Cosmochim. Acta* **48**, 2651–2658.

Kemper F., Vriend W. J. and Tielens A. G. G. M. (2004) The absence of crystalline silicates in the diffuse interstellar medium. *Astrophys. J. Lett.* **609**, 826–837.

Kennicutt, Jr., R. C. and Evans, II, N. J. (2012) Star formation in the Milky Way and nearby galaxies. *Ann. Rev. Astron. Astrophys.* **50**, 531–608.

Kleine T., Touboul M., Bourdon B., Nimmo F., Mezger K., Palme H., Jacobsen S. B., Yin Q.-Z. and Halliday A. N. (2009) Hf–W chronology of the accretion and early evolution of asteroids and terrestrial planets. *Geochim. Cosmochim. Acta* **73**, 5150–5188.

Krot A. N., Amelin Y., Bland P., Ciesla F. J., Connelly J., Davis A. M., Huss G. R., Hutcheon I. D., Makide K., Nagashima K., Nyquist L. E., Russell S. S., Scott E. R. D., Thrane K., Yurimoto H. and Yin Q.-Z. (2009) Origin and chronology of chondritic components: A review. *Geochim. Cosmochim. Acta* **73**, 4963–4997.

Krot A. N., Nagashima K., Wasserburg G. J., Huss G. R., Papanastassiou D., Davis A. M., Hutcheon I. D. and Bizzarro M. (2014) Calcium-aluminum-rich inclusions with fractionation and unknown nuclear effects (FUN CAIs): I. Mineralogy, petrology, and oxygen isotopic compositions. *Geochim. Cosmochim. Acta* **143**, 206–247.

Larsen K. K., Trinquier A., Paton C., Schiller M., Wielandt D., Ivanova M. A., Connelly J. N., Nordlund Å., Krot A. N. and Bizzarro M. (2011) Evidence for magnesium isotope heterogeneity in the solar protoplanetary disk. *Astrophys. J. Lett.* **735**, L37.

Lee T., Papanastassiou D. and Wasserburg G. (1977) Al-26 in the early solar-system – Fossil or fuel. *Astrophys. J.* **211**, L107–L110.

Lee T., Papanastassiou D. A. and Wasserburg G. J. (1978) Calcium isotopic anomalies in the Allende meteorite. *Astrophys. J.* **220**, L21–L25.

Lee T., Russell W. and Wasserburg G. (1979) Calcium isotopic anomalies and the lack of Al-26 in an unusual Allende inclusion. *Astrophys. J.* **228**, L93–L98.

Liu M.-C., McKeegan K. D., Goswami J. N., Marhas K. K., Sahijpal S., Ireland T. R. and Davis A. M. (2009) Isotopic records in CM Hibonites: Implications for timescales of mixing of isotope reservoirs in the solar nebula. *Geochim. Cosmochim. Acta* **73**, 5051–5079.

Liu M.-C., Chaussidon M., Srinivasan G. and McKeegan K. D. (2012) A lower initial abundance of short-lived ^{41}Ca in the early solar system and its implications for solar system formation. *Astrophys. J.* **761**, 137.

Lugaro M., Heger A., Osrin D., Goriely S., Zuber K., Karakas A. I., Gibson B. K., Doherty C. L., Lattanzio J. C. and OTT U. (2014) Stellar origin of the ^{182}Hf cosmochronometer and the presolar history of solar system matter. *Science* **345**, 650–653.

Matsuura M., Dwek E., Meixner M., Otsuka M., Babler B., Barlow M. J., Roman-Duval J., Engelbracht C., Sandstrom K., Lakicevic M., van Loon J. T., Sonneborn G., Clayton G. C., Long K. S., Lundqvist P., Nozawa T., Gordon K. D., Hony S., Panuzzo P., Okumura K., Misselt K. A., Montiel E. and Sauvage M. (2011) Herschel detects a massive dust reservoir in supernova 1987A. *Science* **333**, 1258–1261.

Matzner C. D. (2002) On the role of massive stars in the support and destruction of giant molecular clouds. *Astrophys. J.* **566**, 302–314.

Meyer B. S., Krishnan T. D. and Clayton D. D. (1996) ^{48}Ca production in matter expanding from high temperature and density. *Astrophys. J.* **462**, 825.

Moynier F., Simon J. I., Podosek F. A., Meyer B. S., Brannon J. and DePaolo D. J. (2010) Ca isotope effects in Orgueil leachates and the implications for the carrier phases of Cr-54 anomalies. *Astrophys. J. Lett.* **718**, L7–L13.

Murray N. (2011) Star formation efficiencies and lifetimes of giant molecular clouds in the Milky Way. *Astrophys. J. Lett.* **729**, 133.

Niederer F. R. and Papanastassiou D. (1984) Ca isotopes in refractory inclusions. *Geochim. Cosmochim. Acta* **48**, 1279–1293.

Nittler L. R., Amari S., Zinner E., Woosley S. E. and Lewis R. S. (1996) Extinct ^{44}Ti in presolar graphite and SiC: Proof of a supernova origin. *Astrophys. J. Lett.* **462**, L31.

Önehag A., Korn A., Gustafsson B., Stempels E. and VandenBerg D. A. (2011) M67-1194, an unusually sun-like solar twin in M67. *Astron. Astrophys.* **528**, A85.

Paton C., Hellstrom J., Paul B., Woodhead J. and Hergt J. (2011) Iolite: Freeware for the visualisation and processing of mass spectrometric data. *J. Anal. At. Spectrom.* **26**, 2508.

Paton C., Schiller M. and Bizzarro M. (2013) Identification of an ^{84}Sr-depleted carrier in primitive meteorites and implications for thermal processing in the solar protoplanetary disk. *Astrophys. J.* **763**, L40.

Podosek F., Ott U., Brannon J., Neal C., Bernatowicz T. J., Swan P. and Mahan S. E. (1997) Thoroughly anomalous CR in Orgueil. *Meteoritics* **32**, 617–627.

Qin L., O'D Alexander C. M., Carlson R. W., Horan M. F. and Yokoyama T. (2010) Contributors to chromium isotope variation of meteorites. *Geochim. Cosmochim. Acta* **74**, 1122–1145.

Qin L., Carlson R. W. and Alexander C. M. O. (2011a) Correlated nucleosynthetic isotopic variability in Cr, Sr, Ba, Sm, Nd and Hf in Murchison and QUE 97008. *Geochim. Cosmochim. Acta* **75**, 7806–7828.

Qin L., Nittler L. R., Alexander C. M. O., Wang J., Stadermann F. J. and Carlson R. W. (2011b) Extreme ^{54}Cr-rich nano-oxides in the CI chondrite Orgueil – Implication for a late supernova injection into the solar system. *Geochim. Cosmochim. Acta* **75**, 629–644.

Rauscher T., Heger A., Hoffman R. D. and Woosley S. E. (2002) Nucleosynthesis in massive stars with improved nuclear and stellar physics. *Astrophys. J.* **576**, 323–348.

Reisberg L., Dauphas N., Luguet A., Pearson D. G., Gallino R. and Zimmermann C. (2009) Nucleosynthetic osmium isotope anomalies in acid leachates of the Murchison meteorite. *Earth Planet. Sci. Lett.* **277**, 334–344.

Rotaru M., Birck J.-L. and Allègre C. J. (1992) Clues to early solar system history from chromium isotopes in carbonaceous chondrites. *Nature* **358**, 465–470.

Russell W., Papanastassiou D. and Tombrello T. A. (1978) Ca isotope fractionation on earth and other solar-system materials. *Geochim. Cosmochim. Acta* **42**, 1075–1090.

Sahijpal S. and Goswami J. N. (1998) Refractory phases in primitive meteorites devoid of ^{26}Al and ^{41}Ca: Representative samples of first solar system solids? *Astrophys. J. Lett.* **509**, L137.

Schiller M., Baker J. A. and Bizzarro M. (2010) ^{26}Al–^{26}Mg dating of asteroidal magmatism in the young solar system. *Geochim. Cosmochim. Acta* **74**, 4844–4864.

Schiller M., Paton C. and Bizzarro M. (2012) Calcium isotope measurement by combined HR-MC-ICPMS and TIMS. *J. Anal. At. Spectrom.* **27**, 38–49.

Simon J. I., DePaolo D. J. and Moynier F. (2009) Calcium isotope composition of meteorites, Earth, and Mars. *Astrophys. J.* **702**, 707–715.

Srinivasan G., Ulyanov A. and Goswami J. (1994) ^{41}Ca in the early solar system. *Astrophys. J.* **431**, L67–L70.

Steele R. C. J., Coath C. D., Regelous M., Russell S. and Elliott T. (2012) Neutron-poor nickel isotope anomalies in meteorites. *Astrophys. J.* **758**, 59.

Tang H. and Dauphas N. (2012) Abundance, distribution, and origin of ^{60}Fe in the solar protoplanetary disk. *Earth Planet. Sci. Lett.*, 248–263.

Thrane K., Nagashima K., Krot A. N. and Bizzarro M. (2008) Discovery of a new FUN CAI from a CV carbonaceous chondrite: Evidence for multistage thermal processing in the protoplanetary disk. *Astrophys. J. Lett.* **680**, L141–L144.

Trinquier A., Birck J.-L. and Allegre C. (2007) Widespread Cr-54 heterogeneity in the inner solar system. *Astrophys. J.* **655**, 1179–1185.

Trinquier A., Birck J.-L., Allègre C. J., Gopel C. and Ulfbeck D. (2008) ^{53}Mn–^{53}Cr systematics of the early solar system revisited. *Geochim. Cosmochim. Acta* **72**, 5146–5163.

Trinquier A., Elliott T., Ulfbeck D., Coath C., Krot A. and Bizzarro M. (2009) Origin of nucleosynthetic isotope heterogeneity in the solar protoplanetary disk. *Science* **324**, 374–376.

Valdes M. C., Moreira M., Foriel J. and Moynier F. (2014) The nature of Earth's building blocks as revealed by calcium isotopes. *Earth Planet. Sci. Lett.* **394**, 135–145.

Vasileiadis A., Nordlund Å. and Bizzarro M. (2013) Abundance of ^{26}Al and ^{60}Fe in evolving giant molecular clouds. *Astrophys. J.* **769**, L8.

Wallerstein G., Iben I. J., Parker P., Boesgaard A. M., Hale G. M., Champagne A. E., Barnes C. A., Käppeler F., Smith V. V., Hoffman R. D., Timmes F. X., Sneden C., Boyd R. N., Meyer B. S. and Lambert D. L. (1997) Synthesis of the elements in stars: Forty years of progress. *Rev. Mod. Phys.* **69**, 995–1084.

Wanajo S., Nomoto K., Janka H. T., Kitaura F. S. and Müller B. (2009) Nucleosynthesis in electron capture supernovae of asymptotic giant branch stars. *Astrophys. J. Lett.* **695**, 208–220.

Wanajo S., Janka H.-T. and Müller B. (2013) Electron-capture supernovae as origin of ^{48}Ca. *Astrophys. J.* **767**, L26.

Wasserburg G. J., Lee T. and Papanastassiou D. (1977) Correlated O and Mg isotopic anomalies in Allende inclusions. II – Magnesium. *Geophys. Res. Lett.* **4**, 299–302.

Wasserburg G. J., Wimpenny J. and Yin Q.-Z. (2012) Mg isotopic heterogeneity, Al–Mg isochrons, and canonical ^{26}Al/^{27}Al in the early solar system. *Meteorit. Planet. Sci.* **47**, 1980–1997.

Wombacher F. and Rehkämper M. (2003) Investigation of the mass discrimination of multiple collector ICP-MS using neodymium isotopes and the generalised power law. *J. Anal. At. Spectrom.* **18**, 1371.

Woosley S. (1997) Neutron-rich nucleosynthesis in carbon deflagration supernovae. *Astrophys. J.* **476**, 801–810.

Woosley S. E. and Weaver T. A. (1995) The evolution and explosion of massive stars. II. Explosive hydrodynamics and nucleosynthesis. *Astrophys. J. Suppl.* **101**, 181–235.

Zhang J., Dauphas N., Davis A. M. and Pourmand A. (2011) A new method for MC-ICPMS measurement of titanium isotopic composition: Identification of correlated isotope anomalies in meteorites. *J. Anal. At. Spectrom.* **26**, 2197–2205.

Zhang J., Huang S., Davis A. M., Dauphas N., Hashimoto A. and Jacobsen S. B. (2014) Calcium and titanium isotopic fractionations during evaporation. *Geochim. Cosmochim. Acta* **140**, 365–380.

Zinner E. (2007) Presolar grains. In *Treatise on Geochemistry*. Elsevier, pp. 1–33.

Zinner E., Nittler L., Hoppe P., Gallino R., Straniero O. and Alexander C. (2005) Oxygen, magnesium and chromium isotopic ratios of presolar spinel grains. *Geochim. Cosmochim. Acta* **69**, 4149–4165.

Associate editor: Shichun Huang